

Large impact of phonon lineshapes on the superconductivity of solid hydrogen

Đorđe Dangić,^{1,2,*} Lorenzo Monacelli,³ Raffaello Bianco,^{4,5,6} Francesco Mauri,⁷ and Ion Errea^{1,2,8}

¹*Fisika Aplikatua Saila, Gipuzkoako Ingeniaritza Eskola,*

University of the Basque Country (UPV/EHU), Europa Plaza 1, 20018 Donostia/San Sebastián, Spain

²*Centro de Física de Materiales (CSIC-UPV/EHU),*

Manuel de Lardizabal Pasealekua 5, 20018 Donostia/San Sebastián, Spain

³*Theory and Simulation of Materials (THEOS), École Polytechnique Fédérale de Lausanne, CH-1015 Lausanne, Switzerland*

⁴*Ruder Bošković Institute, 10000 Zagreb, Croatia*

⁵*Dipartimento di Scienze Fisiche, Informatiche e Matematiche,*

Università di Modena e Reggio Emilia, Via Campi 213/a I-41125 Modena, Italy

⁶*Centro S3, Istituto Nanoscienze-CNR, Via Campi 213/a, I-41125 Modena, Italy*

⁷*University of Rome, "Sapienza", Dipartimento di Fisica, Piazzale Aldo Moro 5, 00185, Rome, Italy*

⁸*Donostia International Physics Center (DIPC),*

Manuel de Lardizabal Pasealekua 4, 20018 Donostia/San Sebastián, Spain

(Dated: April 6, 2023)

Phonon anharmonicity plays a crucial role in determining the stability and vibrational properties of high-pressure hydrides. Furthermore, strong anharmonicity can render phonon quasiparticle picture obsolete. In this work, we show the effects of non-Lorentzian phonon lineshapes on the superconductivity of high-pressure solid hydrogen. We calculate the superconducting critical temperature T_C *ab initio* considering the full anharmonic lineshape of the phonon spectral function and show that it substantially enhances T_C . Despite previous anharmonic calculations estimating a weak anharmonicity in atomic hydrogen, considering the full spectral function enhances the critical temperature by 100 K, pushing it above 400 K. Our calculations also reveal that superconductivity emerges in hydrogen in the Cmca-12 molecular phase VI at pressures between 450 and 500 GPa.

Solid atomic hydrogen was postulated to be a high-temperature superconductor at high pressures by Ashcroft in 1968 [1]. Later this idea has been revised and hydrogen-rich compounds have been hypothesized to be high-temperature superconductors at pressures that are only a fraction of the one needed to get atomic hydrogen [2, 3]. The first experimental verification of that idea came in 2015 when H_3S was shown to have a transition temperature of 203 K at 155 GPa [4]. This has been followed up by numerous experiments on different hydrogen compounds, many of them exhibiting high-temperature superconductivity [5–11], verifying without a reasonable doubt the existence of superconductivity in hydrides at high pressures [12].

The discovery of high-temperature superconductivity renewed the interest in synthesizing atomic metallic hydrogen, which is expected to superconduct above room temperature [13–16]. Recently, a work reported atomic metallic hydrogen at 495 GPa on the basis of enhanced optical reflectivity [17]. While this finding was questioned [18] due to a probable overestimation of the measured pressure, there is an abundant amount of proof of metalization of solid hydrogen in the molecular phase [19, 20]. None of these works, however, observed the transition to the superconducting phase up to 440 GPa [21].

A better understanding of the high-pressure solid hydrogen phase diagram was provided by recent first-principles calculations considering both electronic correlations beyond density functional theory (DFT) and nuclear quantum effects [22–24]. Monacelli et al. show that

at pressures lower than 422 GPa hydrogen crystallizes in the C2/c-24 phase, with 24 atoms in the primitive unit cell (phase III of solid hydrogen). In a pressure range between 422 and 577 GPa hydrogen transforms to the Cmca-12 phase, with 12 atoms per unit cell (phase VI). The value of 422 GPa agrees very well with the experimental transition pressures detected by infrared at 420 GPa [20] and by Raman at 440 GPa [19]. Finally, at pressures higher than 577 GPa, hydrogen transforms into atomic hydrogen with a tetragonal $I4_1/amd-2$ structure, containing two atoms per primitive unit cell.

One of the key reasons why studies in Refs. [22, 23] were able to successfully model the phase diagram of solid hydrogen was the inclusion of quantum anharmonic effects. The phonon renormalization due to anharmonicity can significantly alter superconductivity, as shown in Refs. [25–29]. However, these studies have not explored the anharmonicity-induced dynamical renormalization of phonons and its impact on superconductivity. Some studies have highlighted the importance of these effects on superconductivity utilizing simple single phonon mode toy models [30, 31]. On the other hand, dynamical renormalization of phonons due to electron-phonon coupling has been shown to have little impact on the critical temperature [32] of conventional superconductors. However, the dynamical effects due to phonon-phonon interaction should be much stronger in high-pressure hydrides, and thus a full first principle study of these effects is necessary.

Here we present a first-principles study of the superconducting properties of solid hydrogen in its high-

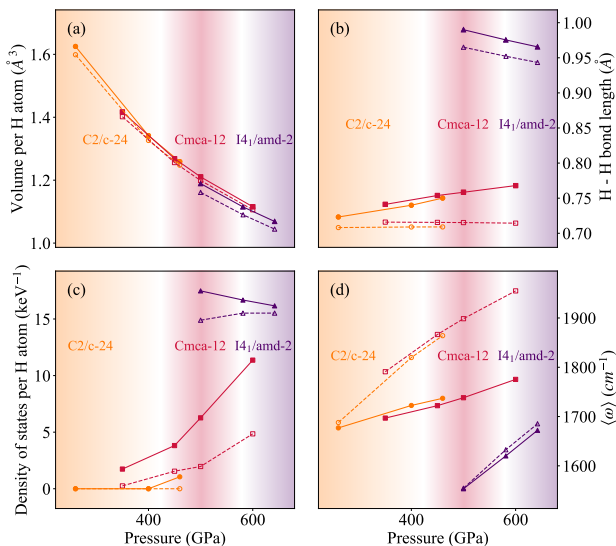


FIG. 1. (a) Volume of the primitive unit cell per hydrogen atom, (b) length of the hydrogen-hydrogen bond, (c) the electronic DOS at the Fermi level per hydrogen atom and (d) the average phonon frequency in high-pressure solid hydrogen. Solid lines represent data obtained with SSCHA and dashed lines with the harmonic approximation. The color background shows a phase diagram of the solid hydrogen from Ref. [23] and the color of the lines indicate for which phase calculations were performed.

pressure phases from 300 to 600 GPa by accounting for quantum anharmonic effects both on the phonons and the structure with the stochastic self-consistent harmonic approximation (SSCHA) at zero Kelvin [33]. We find that the SSCHA appreciably changes the structure of solid hydrogen in all phases, which leads to an increased density of states (DOS) at the Fermi level and an overall phonon softening. These two effects combine to increase the electron-phonon coupling constants and superconducting transition temperatures in the SSCHA structures, at odds with previous calculations that neglect the impact of ionic quantum effects on the structure [28, 29]. We also show that the phonon spectral functions of all these phases have a complex and broad shape, clearly deviating from a simple Lorentzian, questioning the standard approximation made in the electron-phonon calculations in which the spectral function is represented with a Dirac delta function. By considering the full spectral function for the first time ever, we show that the critical temperature (T_C) of both molecular and atomic phases is considerably enhanced, especially for the latter, where the critical temperature is boosted above 400 K. Our calculations predict the onset of superconductivity in solid hydrogen in the semimetallic molecular phase VI at pressures between 450 and 500 GPa, in agreement with recent experiments [19].

Quantum anharmonic effects have a large impact on

the structures in the phase diagram as shown in Fig. 1. There is a discontinuity in volume at the phase transition between molecular and atomic phases, not evident for the transition between molecular phases III and VI. This discontinuity is partly suppressed in the quantum anharmonic SSCHA structures. The SSCHA expands the structure slightly for all phases, most prominently for the atomic phase, increasing bond lengths and the c/a ratio at all pressures, as it has been already calculated in other high-pressure hydrides [34, 35]. Importantly, SSCHA changes the qualitative behavior of bond lengths in molecular phases: while in SSCHA the bond length increases with pressure, in the harmonic approximation it stays relatively constant [22].

These changes have a significant effect on the electronic and vibrational properties of solid hydrogen (see Figs. 1 and 2). The most prominent impact is the increase of the DOS at the Fermi level in the quantum anharmonic SSCHA structures. In the molecular phase VI, decreasing volume leads to an increase in the DOS, but with a considerably higher slope for the SSCHA structures than for the harmonic ones. This behavior shows that quantum anharmonic effects tend to increase the DOS at the Fermi level, as already described in several hydrides [35, 36]. Molecular phase III is only weakly semimetallic up to 450 GPa and will not be discussed further on, as, thus, it cannot superconduct despite prior claims [29]. Closing of the fundamental band gap in our calculations occurs above 400 GPa, which is slightly overestimated compared to calculations that include both better approximation for the exchange-correlation functional and the effect of the electron-phonon coupling [22, 24].

In addition to the structure modified by quantum nuclear effects, SSCHA method allows us to obtain second-order force constants renormalized by anharmonicity. Quantum anharmonicity softens phonon frequencies as a consequence of the stretching of the H bonds (see Fig. 1). This is at odds with recent calculations [28, 29], in which the frequencies of the phonon modes excluding the vibrons increase due to anharmonicity. The difference is that in the latter case the effect of the quantum zero-point fluctuations on the structure was neglected, which our calculations show to be important. Both the increase of the DOS at the Fermi level and the phonon softening are beneficial for superconductivity since the electron-phonon coupling constant scales inversely with phonon frequencies and linearly with the DOS at the Fermi level.

Beyond the renormalization of structural parameters and phonon frequencies, anharmonicity has a huge impact on the phonon spectral function (see Supplementary Material for more details [33]). The spectral function of all phases shows further softening with respect to the auxiliary SSCHA phonon frequencies, especially for high-frequency optical modes. More remarkably, even at vanishing temperatures, we predict a huge broadening of the phonon spectral functions, clearly deviating from

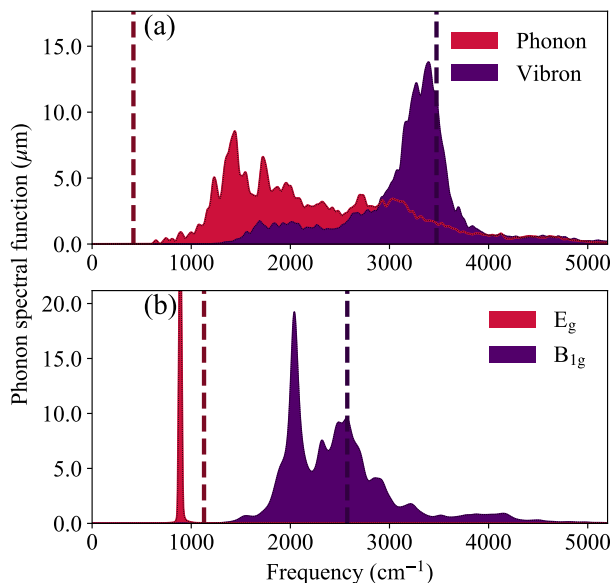


FIG. 2. Phonon spectral functions in the no mode mixing approximation in mode basis, $\sigma_\mu(\mathbf{q}, \omega)$, of two representative optical phonon modes at Γ of solid hydrogen in (a) molecular Cmca-12 phase VI at 500 GPa, and (b) atomic tetragonal $I4_1/amd-2$ phase at 500 GPa. In figure (b) we scaled the values of the E_g mode in order to make the figures clearer. Thick dashed vertical lines represent the corresponding frequencies obtained from the auxiliary SSCHA force constants.

the standard Lorentzian line shape. We illustrate this in Fig. 2, where phonon spectral functions for selected modes at Γ point are presented for structures at 500 GPa in molecular phase VI and atomic phase. We report two representative modes for molecular phase VI: a global lattice vibration (phonon mode) and a stretching of H_2 molecule (vibron mode). In the atomic phase, we only have two optical modes that are non-degenerate and we show both of them. The shift of the phonon frequency is very large in all cases. Additionally, all modes, except the E_g one in the atomic phase, have a huge broadening of the phonon spectral function of thousands of cm^{-1} and a clear non-Lorentzian line shape. Such anomalous behavior questions the standard practice of approximating the spectral function with slightly smeared Delta functions in first-principles calculations of the superconducting critical temperatures. In fact, it has already been shown that non-Lorentzian lineshapes can have a non-negligible effect on other properties of materials, i.e. the lattice thermal conductivity in highly anharmonic semiconducting chalcogenides [37].

The isotropic Eliashberg function of the electron-phonon interaction can be calculated keeping the full an-

harmonic spectral function as [38]

$$\alpha^2 F(\omega) = \frac{1}{N_{\mathbf{q}}} \sum_{ab\mathbf{q}} \frac{\Delta^{ab}(\mathbf{q})\sigma_{ab}(\mathbf{q}, \omega)}{\omega\sqrt{m_a m_b}}, \quad (1)$$

where $\sigma_{ab}(\mathbf{q}, \omega)$ is the phonon spectral function in the Cartesian basis with wave number \mathbf{q} (see Supplementary Material for more details [33]). In Eq. (1) a and b label both atoms and a Cartesian direction, $\Delta^{ab}(\mathbf{q})$ represents the average of the deformation potential over the Fermi surface, m_a is the mass of atom a , and $N_{\mathbf{q}}$ is the number of \mathbf{q} points in the sum. In the harmonic case, this quantity is calculated for the structure that minimizes the BOES, while in the SSCHA it is calculated for the structure that minimizes the free energy.

All calculations thus far that have accounted for anharmonicity in the calculation of $\alpha^2 F(\omega)$ have been performed assuming that $\sigma_{ab}(\mathbf{q}, \omega)$ can be expressed as [15, 25–27, 35, 36] $\sigma_{ab}(\mathbf{q}, \omega) = \sum_{\mu} e_{\mu}^a(\mathbf{q})e_{\mu}^{b*}(\mathbf{q})\sigma_{\mu}^h(\mathbf{q}, \omega)$, where the harmonic spectral function $\sigma_{\mu}^h(\mathbf{q}, \omega)$ of mode μ and wave number \mathbf{q} is a Delta function centered at the harmonic or SSCHA auxiliary phonon frequency, and $e_{\mu}(\mathbf{q})$ are either harmonic or SSCHA phonon eigenvectors. As in practical implementations, the Delta functions are numerically approximated with a Gaussian function of fixed spread, we label this approach as *Gaussian*.

However, as we have shown in Fig. 2, anharmonicity can drastically affect the phonon lineshapes. Using the same projection method one can obtain $\sigma_{ab}(\mathbf{q}, \omega) = \sum_{\mu} e_{\mu}^a(\mathbf{q})e_{\mu}^{b*}(\mathbf{q})\sigma_{\mu}(\mathbf{q}, \omega)$, where $\sigma_{\mu}(\mathbf{q}, \omega)$ are the diagonal phonon spectral functions calculated in the *no-mode mixing* approximation accounting for the phonon-phonon interaction in the dynamical bubble approximation (see Supplementary Material for more details). The polarization vectors used in the projection, in this case, are those obtained from the SSCHA auxiliary dynamical matrices. By calculating $\alpha^2 F(\omega)$ with the $\sigma_{ab}(\mathbf{q}, \omega)$ in the no-mode mixing approximation, we see that the anharmonic spectral function has a huge impact, as shown in Fig. 3. The softening of the phonon modes is also evident in the Eliashberg spectral functions. Additionally, the broadening of the phonon lineshapes leads to the complete closing of the gap between hydrogen vibron and phonon branches in the molecular phase VI. The softening of the phonon modes in the SSCHA coupled with a higher DOS at the Fermi level in the SSCHA structures leads to higher values of the electron-phonon coupling constant λ in most cases compared to the harmonic result, more remarkably in the molecular phase VI. A notable exception is atomic hydrogen at 500 GPa, where the proximity to a phonon instability, which is suppressed by anharmonicity, drastically increases λ in the harmonic approximation (see Supplementary Material [33]).

The no-mode mixing approximation describes the phonon lineshapes very well [39] and is used almost ex-

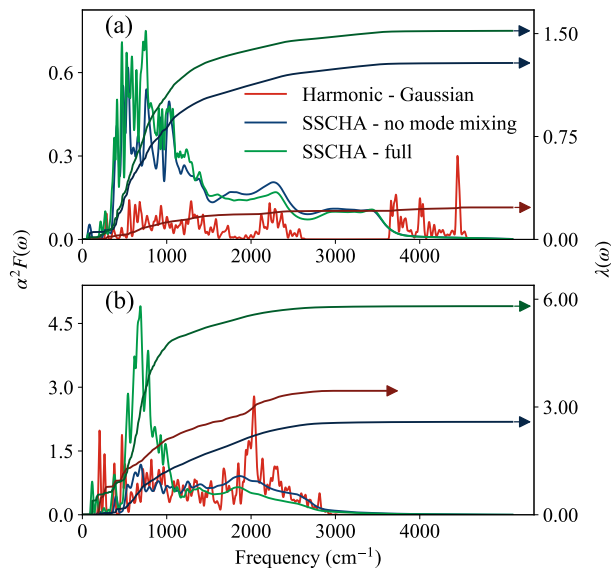


FIG. 3. Eliashberg spectral function $\alpha^2 F(\omega)$ and integrated electron-phonon coupling constant $\lambda(\omega)$ of solid hydrogen in (a) molecular Cmca-12 phase VI at 500 GPa, and (b) atomic tetragonal $I4_1/amd-2$ phase at 500 GPa calculated in the SSCHA using the spectral function calculated fully and in the no mode mixing approximation, and in the harmonic case using Gaussian method.

clusively when discussing the anharmonic phonon line-shapes. However, we can go one step further and utilize the full spectral function without limiting ourselves to the standard no-mode mixing approximation. In this case, we do not assume that the phonon self-energy is diagonal in the phonon branch index, as it is done in the no-mode mixing case, and instead calculate the spectral function as $\sigma_{ab}(\mathbf{q}, \omega) = \sum_{\mu\nu} e_{\mu}^a(\mathbf{q}) e_{\nu}^{b*}(\mathbf{q}) \sigma_{\mu\nu}(\mathbf{q}, \omega)$ fully accounting for off-diagonal terms, where again the polarization vectors are obtained from the SSCHA auxiliary dynamical matrices (see Supplementary Material [33]). The Eliashberg spectral functions in this approach have stronger spectral weights for frequencies near 1000 cm^{-1} compared to the no-mode mixing approximation, especially in the atomic phase (see Fig. 3), which increases the electron-phonon coupling constant and T_C . On the other hand, the phonon density of states calculated with the two methods (see Supplementary Material) are almost identical. Hence, the reason for the increase in the Eliashberg spectral function is nuanced and depends on the redistribution of spectral weights when the full spectral function is considered. These changes might be detected in experiments, at least in the atomic phase, as they could lead to qualitative changes in the reflectivity of the material [40], while the enhancement of λ is large enough to be experimentally resolved [41]. For comparison, we have checked that in the high- T_C superconducting H_3S the Gaussian, no-mode mixing and full

spectral functions calculations yield similar results (see Supplementary Material), indicating that the large enhancement of λ observed in hydrogen by the full spectral function is system dependent and not universal.

Solving isotropic Migdal-Eliashberg equations with the $\alpha^2 F(\omega)$ obtained considering the full spectral function [38, 42], we can estimate the impact of anharmonicity on the superconducting transition temperature (see Fig. 4). As mentioned above, the C2/c-24 phase of solid hydrogen does not exhibit superconducting behavior in the pressure range of interest. In the molecular phase VI the transition temperature is mostly linear with pressure and correlates well with the value of the DOS at the Fermi level. Because of this, the SSCHA structures consistently show higher transition temperatures than the classical harmonic ones. The difference in T_C between these two methods increases with pressure, again due to the stronger dependence of the electronic DOS on the pressure in the SSCHA structures (see Fig. 1), as well as due to the increased electron-phonon coupling due to the anharmonic softening of the phonon modes. Using the full spectral function increases T_C by around 60 K compared to the standard Gaussian approximation for SSCHA structures. Considering the critical dependence of T_C on the DOS at the Fermi level and that local exchange-correlation functionals tend to overestimate it [13, 15, 28, 29, 43, 44], we perform DFT calculations for the quantum SSCHA structures of phase VI using the B3LYP hybrid functional [45] (see Supplementary Material [33]), which yields the values in Fig. 4. We estimate thus that superconductivity will emerge in solid hydrogen in this phase between 450 and 500 GPa.

The critical temperature is mostly constant with pressure in the atomic tetragonal phase. In this phase, T_C is mostly decorrelated with the value of the electronic DOS at the Fermi level because the structures are far away from the metal-insulator phase transition [23] and, despite quantum and anharmonic effects enhance the DOS as well, its relative increase is small compared to the molecular case. Including the full spectral function in the calculation of $\alpha^2 F(\omega)$ increases the critical temperature significantly, about 100 K for all pressures compared to the Gaussian approximation. This highlights the important role that anharmonicity plays in the superconductivity of high-pressure hydrogen also in the atomic phase, contrary to the previous calculations that only estimated its effect within the Gaussian approximation of the spectral function [15].

In conclusion, our first-principles calculations considering ionic quantum effects and anharmonicity show that superconductivity will emerge in solid hydrogen in molecular phase VI, between 450 and 500 GPa, and T_C will rapidly soar with pressure. We expect a jump of T_C to approximately 400 K at the transition to the atomic phase. Quantum anharmonic effects have a huge impact on the structural, vibrational, and superconducting prop-

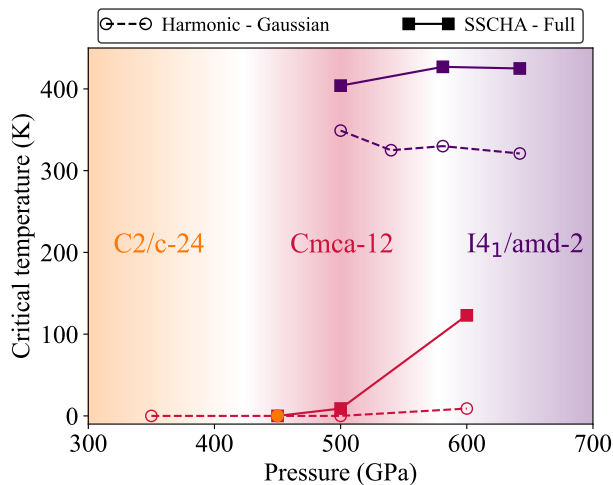


FIG. 4. Calculated superconducting transition temperature in solid hydrogen in different phases and pressures within the SSCHA using the full phonon spectral functions (full symbols and solid lines) and the harmonic approximation using Gaussian method (empty symbols and dashed lines). Shaded regions represent the phase diagram of solid hydrogen from Ref. [23]. Line colors denote for which phase calculations were performed (red for molecular phase VI and purple for atomic phase).

erties of both molecular and atomic phases by, for instance, increasing the H-H bonds and making the phonon spectral functions extremely broad and anomalous. We show that considering the full phonon spectral function in the calculation of $\alpha^2F(\omega)$ enhances the predicted critical temperature by 100 K in the atomic phase and 60 K in the molecular phase VI.

This work is supported by the European Research Council (ERC) under the European Unions Horizon 2020 research and innovation program (grant agreement No. 802533) and the Department of Education, Universities and Research of the Eusko Jaurlaritza and the University of the Basque Country UPV/EHU (Grant No. IT1527-22). L.M. acknowledges the European Union MSCA-IF fellowship for funding the project THERMOH. We acknowledge PRACE for awarding us access to Joliot-Curie Rome at TGCC, France.

* dorde.dangic@ehu.es

- [1] N. W. Ashcroft, Metallic hydrogen: A high-temperature superconductor?, *Phys. Rev. Lett.* **21**, 1748 (1968).
- [2] N. W. Ashcroft, Hydrogen dominant metallic alloys: High temperature superconductors?, *Phys. Rev. Lett.* **92**, 187002 (2004).
- [3] D. Duan, Y. Liu, F. Tian, D. Li, X. Huang, Z. Zhao, H. Yu, B. Liu, W. Tian, and T. Cui, Pressure-induced

metallization of dense (h2s)2h2 with high- t_c superconductivity, *Scientific Reports* **4**, 6968 (2014).

- [4] A. P. Drozdov, M. I. Eremets, I. A. Troyan, V. Ksenofontov, and S. I. Shylin, Conventional superconductivity at 203 kelvin at high pressures in the sulfur hydride system, *Nature* **525**, 73 (2015).
- [5] A. P. Drozdov, P. P. Kong, V. S. Minkov, S. P. Besedin, M. A. Kuzovnikov, S. Mozaffari, L. Balicas, F. F. Balakirev, D. E. Graf, V. B. Prakapenka, E. Greenberg, D. A. Knyazev, M. Tkacz, and M. I. Eremets, Superconductivity at 250 k in lanthanum hydride under high pressures, *Nature* **569**, 528 (2019).
- [6] M. Somayazulu, M. Ahart, A. K. Mishra, Z. M. Geballe, M. Baldini, Y. Meng, V. V. Struzhkin, and R. J. Hemley, Evidence for superconductivity above 260 k in lanthanum superhydride at megabar pressures, *Phys. Rev. Lett.* **122**, 027001 (2019).
- [7] P. Kong, V. S. Minkov, M. A. Kuzovnikov, A. P. Drozdov, S. P. Besedin, S. Mozaffari, L. Balicas, F. F. Balakirev, V. B. Prakapenka, S. Chariton, D. A. Knyazev, E. Greenberg, and M. I. Eremets, Superconductivity up to 243 k in the yttrium-hydrogen system under high pressure, *Nature Communications* **12**, 5075 (2021).
- [8] L. Ma, K. Wang, Y. Xie, X. Yang, Y. Wang, M. Zhou, H. Liu, X. Yu, Y. Zhao, H. Wang, G. Liu, and Y. Ma, High-temperature superconducting phase in clathrate calcium hydride cah_6 up to 215 k at a pressure of 172 gpa, *Phys. Rev. Lett.* **128**, 167001 (2022).
- [9] I. A. Troyan, D. V. Semenok, A. G. Kvashnin, A. V. Sadakov, O. A. Sobolevskiy, V. M. Pudalov, A. G. Ivanova, V. B. Prakapenka, E. Greenberg, A. G. Gavriluk, I. S. Lyubutin, V. V. Struzhkin, A. Bergara, I. Errea, R. Bianco, M. Calandra, F. Mauri, L. Monacelli, R. Akashi, and A. R. Oganov, Anomalous high-temperature superconductivity in yh_6 , *Advanced Materials* **33**, 2006832 (2021).
- [10] D. V. Semenok, A. G. Kvashnin, A. G. Ivanova, V. Svitlyk, V. Y. Fominski, A. V. Sadakov, O. A. Sobolevskiy, V. M. Pudalov, I. A. Troyan, and A. R. Oganov, Superconductivity at 161 k in thorium hydride $thh10$: Synthesis and properties, *Materials Today* **33**, 36 (2020).
- [11] E. Snider, N. Dasenbrock-Gammon, R. McBride, X. Wang, N. Meyers, K. V. Lawler, E. Zurek, A. Salamat, and R. P. Dias, Synthesis of yttrium superhydride superconductor with a transition temperature up to 262 k by catalytic hydrogenation at high pressures, *Phys. Rev. Lett.* **126**, 117003 (2021).
- [12] M. I. Eremets, V. S. Minkov, A. P. Drozdov, P. P. Kong, V. Ksenofontov, S. I. Shylin, S. L. Bud'ko, R. Prozorov, F. F. Balakirev, D. Sun, S. Mozaffari, and L. Balicas, High-temperature superconductivity in hydrides: Experimental evidence and details, *Journal of Superconductivity and Novel Magnetism* 10.1007/s10948-022-06148-1 (2022).
- [13] J. M. McMahon and D. M. Ceperley, High-temperature superconductivity in atomic metallic hydrogen, *Phys. Rev. B* **84**, 144515 (2011).
- [14] Y. Yan, J. Gong, and Y. Liu, Ab initio studies of superconductivity in monatomic metallic hydrogen under high pressure, *Physics Letters A* **375**, 1264 (2011).
- [15] M. Borinaga, I. Errea, M. Calandra, F. Mauri, and A. Bergara, Anharmonic effects in atomic hydrogen: Superconductivity and lattice dynamical stability, *Phys. Rev. B* **93**, 174308 (2016).

- [16] E. Maksimov and D. Savrasov, Lattice stability and superconductivity of the metallic hydrogen at high pressure, *Solid State Communications* **119**, 569 (2001).
- [17] R. P. Dias and I. F. Silvera, Observation of the wigner-huntington transition to metallic hydrogen, *Science* **355**, 715 (2017).
- [18] A. F. Goncharov and V. V. Struzhkin, Comment on “observation of the wigner-huntington transition to metallic hydrogen”, *Science* **357**, eaam9736 (2017), <https://www.science.org/doi/pdf/10.1126/science.aam9736>.
- [19] M. I. Eremets, A. P. Drozdov, P. P. Kong, and H. Wang, Semimetallic molecular hydrogen at pressure above 350 gpa, *Nature Physics* **15**, 1246 (2019).
- [20] P. Loubeyre, F. Occelli, and P. Dumas, Synchrotron infrared spectroscopic evidence of the probable transition to metal hydrogen, *Nature* **577**, 631 (2020).
- [21] Experimental estimation of the applied pressure depends on different pressure scales used in the community. For this reason, actual pressure exerted on the hydrogen could be lower.
- [22] L. Monacelli, I. Errea, M. Calandra, and F. Mauri, Black metal hydrogen above 360 gpa driven by proton quantum fluctuations, *Nature Physics* **17**, 63 (2021).
- [23] L. Monacelli, M. Casula, K. Nakano, S. Sorella, and F. Mauri, Quantum phase diagram of high-pressure hydrogen (2022).
- [24] V. Gorelov, M. Holzmann, D. M. Ceperley, and C. Pierleoni, Energy gap closure of crystalline molecular hydrogen with pressure, *Phys. Rev. Lett.* **124**, 116401 (2020).
- [25] I. Errea, M. Calandra, C. J. Pickard, J. Nelson, R. J. Needs, Y. Li, H. Liu, Y. Zhang, Y. Ma, and F. Mauri, High-pressure hydrogen sulfide from first principles: A strongly anharmonic phonon-mediated superconductor, *Phys. Rev. Lett.* **114**, 157004 (2015).
- [26] I. Errea, M. Calandra, C. J. Pickard, J. R. Nelson, R. J. Needs, Y. Li, H. Liu, Y. Zhang, Y. Ma, and F. Mauri, Quantum hydrogen-bond symmetrization in the superconducting hydrogen sulfide system, *Nature* **532**, 81 (2016).
- [27] I. Errea, M. Calandra, and F. Mauri, First-principles theory of anharmonicity and the inverse isotope effect in superconducting palladium-hydride compounds, *Phys. Rev. Lett.* **111**, 177002 (2013).
- [28] M. Dogan, S. Oh, and M. L. Cohen, High temperature superconductivity in the candidate phases of solid hydrogen, *Journal of Physics: Condensed Matter* **34**, 15LT01 (2022).
- [29] M. Dogan, S. Oh, and M. L. Cohen, Prediction of high-temperature superconductivity in $c2/c-24$ solid hydrogen, *Phys. Rev. B* **105**, L020509 (2022).
- [30] C. Setty, M. Baggioli, and A. Zaccane, Anharmonic phonon damping enhances the T_c of bcs-type superconductors, *Phys. Rev. B* **102**, 174506 (2020).
- [31] C. Setty, M. Baggioli, and A. Zaccane, Anharmonic theory of superconductivity in the high-pressure materials, *Phys. Rev. B* **103**, 094519 (2021).
- [32] N. Girotto and D. Novko, Dynamical renormalization of electron-phonon coupling in conventional superconductors, *Phys. Rev. B* **107**, 064310 (2023).
- [33] Please see Supplementary Material at XXX for more details on the calculations, the SSCHA theory, and a deeper analysis on the phonon spectra presented here. The Supplementary Material includes citations to Refs. [27, 38, 46–55].
- [34] P. Hou, F. Belli, R. Bianco, and I. Errea, Quantum anharmonic enhancement of superconductivity in p63/mmc sch6 at high pressures: A first-principles study, *Journal of Applied Physics* **130**, 175902 (2021).
- [35] M. Borinaga, P. Riego, A. Leonardo, M. Calandra, F. Mauri, A. Bergara, and I. Errea, Anharmonic enhancement of superconductivity in metallic molecular cmca-4 hydrogen at high pressure: a first-principles study, *Journal of Physics: Condensed Matter* **28**, 494001 (2016).
- [36] I. Errea, F. Belli, L. Monacelli, A. Sanna, T. Koretsune, T. Tadano, R. Bianco, M. Calandra, R. Arita, F. Mauri, and J. A. Flores-Livas, Quantum crystal structure in the 250-kelvin superconducting lanthanum hydride, *Nature* **578**, 66 (2020).
- [37] Đ. Dangić, O. Hellman, S. Fahy, and I. Savić, The origin of the lattice thermal conductivity enhancement at the ferroelectric phase transition in gete, *npj Computational Materials* **7**, 57 (2021).
- [38] P. B. Allen and B. Mitrović, *Theory of superconducting tc* (Academic Press, 1983) pp. 1–92.
- [39] R. Bianco, I. Errea, M. Calandra, and F. Mauri, High-pressure phase diagram of hydrogen and deuterium sulfides from first principles: Structural and vibrational properties including quantum and anharmonic effects, *Phys. Rev. B* **97**, 214101 (2018).
- [40] M. Borinaga, J. Ibañez Azpiroz, A. Bergara, and I. Errea, Strong electron-phonon and band structure effects in the optical properties of high pressure metallic hydrogen, *Phys. Rev. Lett.* **120**, 057402 (2018).
- [41] S. Mozaffari, D. Sun, V. S. Minkov, A. P. Drozdov, D. Knyazev, J. B. Betts, M. Einaga, K. Shimizu, M. I. Eremets, L. Balicas, and F. F. Balakirev, Superconducting phase diagram of h3s under high magnetic fields, *Nature Communications* **10**, 2522 (2019).
- [42] E. R. Margine and F. Giustino, Anisotropic migdaliashberg theory using wannier functions, *Phys. Rev. B* **87**, 024505 (2013).
- [43] P. Cudazzo, G. Profeta, A. Sanna, A. Floris, A. Continenza, S. Massidda, and E. K. U. Gross, Ab initio description of high-temperature superconductivity in dense molecular hydrogen, *Phys. Rev. Lett.* **100**, 257001 (2008).
- [44] P. Cudazzo, G. Profeta, A. Sanna, A. Floris, A. Continenza, S. Massidda, and E. K. U. Gross, Electron-phonon interaction and superconductivity in metallic molecular hydrogen. ii. superconductivity under pressure, *Phys. Rev. B* **81**, 134506 (2010).
- [45] P. J. Stephens, F. J. Devlin, C. F. Chabalowski, and M. J. Frisch, Ab initio calculation of vibrational absorption and circular dichroism spectra using density functional force fields, *The Journal of Physical Chemistry* **98**, 11623 (1994), <https://doi.org/10.1021/j100096a001>.
- [46] S. Baroni, S. de Gironcoli, A. Dal Corso, and P. Giannozzi, Phonons and related crystal properties from density-functional perturbation theory, *Rev. Mod. Phys.* **73**, 515 (2001).
- [47] P. Giannozzi, S. Baroni, N. Bonini, M. Calandra, R. Car, C. Cavazzoni, D. Ceresoli, G. L. Chiarotti, M. Cococcioni, I. Dabo, A. D. Corso, S. de Gironcoli, S. Fabris, G. Fratesi, R. Gebauer, U. Gerstmann, C. Gougoussis, A. Kokalj, M. Lazzeri, L. Martin-Samos, N. Marzari, F. Mauri, R. Mazzarello, S. Paolini, A. Pasquarello, L. Paulatto, C. Sbraccia, S. Scandolo, G. Sclauzero, A. P.

- Seitsonen, A. Smogunov, P. Umari, and R. M. Wentzcovitch, QUANTUM ESPRESSO: a modular and open-source software project for quantum simulations of materials, *Journal of Physics: Condensed Matter* **21**, 395502 (2009).
- [48] P. Giannozzi, O. Andreussi, T. Brumme, O. Bunau, M. B. Nardelli, M. Calandra, R. Car, C. Cavazzoni, D. Ceresoli, M. Cococcioni, N. Colonna, I. Carnimeo, A. D. Corso, S. de Gironcoli, P. Delugas, R. A. DiStasio, A. Ferretti, A. Floris, G. Fratesi, G. Fugallo, R. Gebauer, U. Gerstmann, F. Giustino, T. Gorni, J. Jia, M. Kawamura, H.-Y. Ko, A. Kokalj, E. Küçükbenli, M. Lazzeri, M. Marsili, N. Marzari, F. Mauri, N. L. Nguyen, H.-V. Nguyen, A. O. de-la Roza, L. Paulatto, S. Poncé, D. Rocca, R. Sabatini, B. Santra, M. Schlipf, A. P. Seitsonen, A. Smogunov, I. Timrov, T. Thonhauser, P. Umari, N. Vast, X. Wu, and S. Baroni, Advanced capabilities for materials modelling with quantum ESPRESSO, *Journal of Physics: Condensed Matter* **29**, 465901 (2017).
- [49] B. Miehl, A. Savin, H. Stoll, and H. Preuss, Results obtained with the correlation energy density functionals of Becke and Lee, Yang and Parr, *Chemical Physics Letters* **157**, 200 (1989).
- [50] M. van Setten, M. Giantomassi, E. Bousquet, M. Verstraete, D. Hamann, X. Gonze, and G.-M. Rignanese, The pseudodojo: Training and grading a 85 element optimized norm-conserving pseudopotential table, *Computer Physics Communications* **226**, 39 (2018).
- [51] D. R. Hamann, Optimized norm-conserving Vanderbilt pseudopotentials, *Phys. Rev. B* **88**, 085117 (2013).
- [52] N. Marzari, D. Vanderbilt, A. De Vita, and M. C. Payne, Thermal contraction and disordering of the Al(110) surface, *Phys. Rev. Lett.* **82**, 3296 (1999).
- [53] L. Monacelli, R. Bianco, M. Cherubini, M. Calandra, I. Errea, and F. Mauri, The stochastic self-consistent harmonic approximation: calculating vibrational properties of materials with full quantum and anharmonic effects, *Journal of Physics: Condensed Matter* **33**, 363001 (2021).
- [54] F. Belli, T. Novoa, J. Contreras-García, and I. Errea, Strong correlation between electronic bonding network and critical temperature in hydrogen-based superconductors, *Nature Communications* **12**, 5381 (2021).
- [55] R. Bianco, I. Errea, L. Paulatto, M. Calandra, and F. Mauri, Second-order structural phase transitions, free energy curvature, and temperature-dependent anharmonic phonons in the self-consistent harmonic approximation: Theory and stochastic implementation, *Phys. Rev. B* **96**, 014111 (2017).
- [56] I. Errea, M. Calandra, and F. Mauri, Anharmonic free energies and phonon dispersions from the stochastic self-consistent harmonic approximation: Application to platinum and palladium hydrides, *Phys. Rev. B* **89**, 064302 (2014).
- [57] L. Monacelli, I. Errea, M. Calandra, and F. Mauri, Pressure and stress tensor of complex anharmonic crystals within the stochastic self-consistent harmonic approximation, *Phys. Rev. B* **98**, 024106 (2018).
- [58] L. Monacelli and F. Mauri, Time-dependent self-consistent harmonic approximation: Anharmonic nuclear quantum dynamics and time correlation functions, *Phys. Rev. B* **103**, 104305 (2021).
- [59] J.-M. Lihm and C.-H. Park, Gaussian time-dependent variational principle for the finite-temperature anharmonic lattice dynamics, *Phys. Rev. Research* **3**, L032017 (2021).
- [60] A. Siciliano, L. Monacelli, G. Caldarelli, and F. Mauri, Wigner gaussian dynamics: simulating the anharmonic and quantum ionic motion (2023).

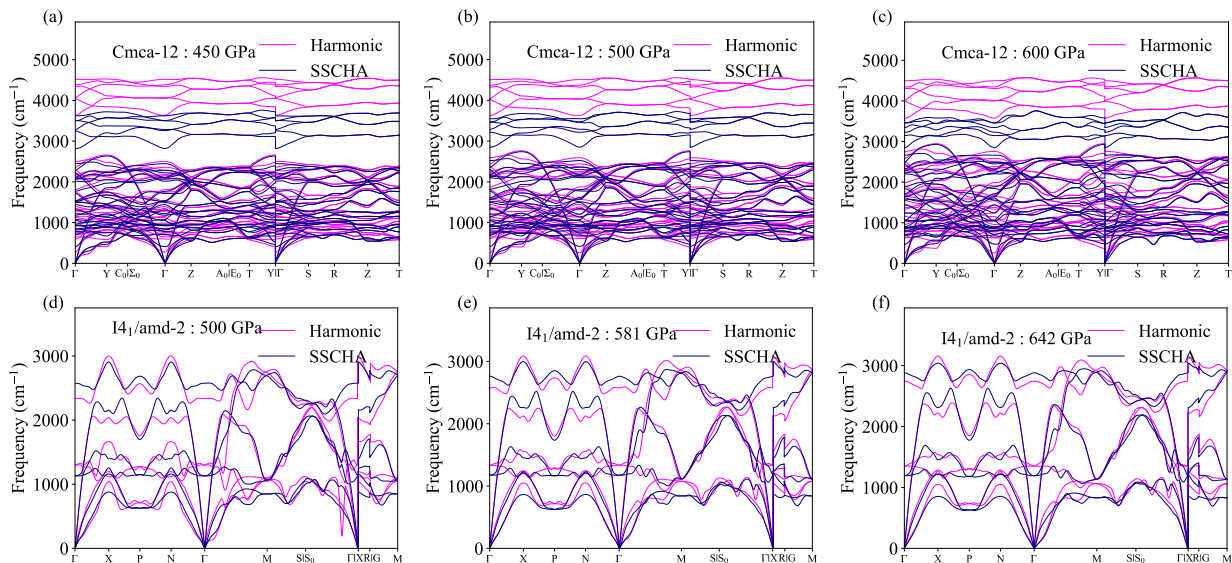
**SUPPLEMENTARY MATERIAL FOR
“LARGE IMPACT OF PHONON LINESHAPES ON THE SUPERCONDUCTIVITY OF SOLID
HYDROGEN”**

Computational details

Density functional theory (DFT) and density functional perturbation theory (DFPT) [46] calculations were performed using Quantum Espresso software [47, 48], implementing the generalized gradient approximation (GGA) with the BLYP parameterization [49] for the exchange-correlation functional. In the case of the primitive unit cell calculations, we used a Monkhorst-Pack grid for sampling electronic states with densities of $48 \times 48 \times 48$ for the atomic phase, $12 \times 12 \times 12$ for the molecular phase VI, and $12 \times 6 \times 12$ for molecular phase III. The electronic wave functions were represented in a plane wave expansion using an 80 Ry energy cutoff (320 Ry cutoff for the electronic density). To describe hydrogen ions we used a norm-conserving pseudo-potential with no pseudized electrons generated by the Pseudo Dojo library [50] and the ONCVSP software [51]. Considering that we are investigating metallic/semimetallic phases we used a Marzari-Vanderbilt smearing of 0.03 Ry [52] for Brillouin zone integrations.

To get the structural and vibrational properties of solid hydrogen we used the stochastic self-consistent harmonic approximation [53]. The sampling of atomic positions and forces was done on a $5 \times 5 \times 5$ primitive cell repetition for the atomic phase, $2 \times 2 \times 2$ for the molecular phase VI, and $2 \times 1 \times 2$ for the molecular phase III. The number of configurations used for the stochastic sampling was 500 for the atomic phase, 600 for molecular phase VI, and 6000 for molecular phase III. To calculate third order force constants needed to calculate the spectral functions we used a finer stochastic sampling of 3000 structures for the atomic phase and 20000 structures for phase VI. SSCHA calculations were performed at 0 K.

Finally, we performed a convergence study of the electron-phonon coupling constant and the critical temperature with respect to the \mathbf{q} point grid in DFPT calculations. We have found that reasonably converged results were obtained with a $12 \times 12 \times 12$ \mathbf{q} point grid for the atomic phase, $8 \times 8 \times 8$ for phase VI, and $8 \times 4 \times 8$ for phase III. The calculated electron-phonon coupling constants from DFPT were projected onto SSCHA phonon modes [27]. \mathbf{k} -point grids for the non-self-consistent calculations for the electron-phonon coupling were done on $100 \times 100 \times 100$ grids for the atomic phase, $44 \times 44 \times 44$ for phase VI, and $44 \times 22 \times 44$ for phase III with a Gaussian smearing of 0.012 Ry for the energy conservation. Finally, to calculate superconducting transition temperatures we used the isotropic approximation of the Migdal-Eliashberg equations [38]. We use $\mu^* = 0.16$ for the Coulomb pseudopotential and a cutoff for the Matsubara frequencies of 0.15 Ha, about 10 times the Debye frequency [38].



Supplementary Figure 1. Phonon band structures for harmonic and SSCHA structures of solid hydrogen in molecular Cmca-12 phase VI at (a) 450 GPa, (b) 500 GPa, (c) 600 GPa, and atomic I₄₁/amd-2 tetragonal phase at (d) 500 GPa, (e) 581 GPa, and (f) 642 GPa. SSCHA phonon spectra are calculated from the auxiliary force constants.

Comparison of harmonic and SSCHA phonon band structures

The SSCHA method [53, 55–57] allows us to minimize the total free energy of the system, which includes the quantum zero point motion and anharmonicity, with respect to two variational parameters that define the ionic wave function: the centroid positions and the auxiliary force constants. The centroids are the average positions of the atoms, the means of the Gaussians that approximate the ionic wave functions. The auxiliary force constants are related to the standard deviation of the Gaussians. Eigenvalues of the dynamical matrices constructed from these auxiliary force constants can be regarded as better estimates of the true phonon frequencies than the simple harmonic force constants since they have been renormalized by anharmonicity. A physically more relevant representation of the vibrational properties of materials comes from the phonon spectral functions obtained in the dynamical dressed-bubble approximation, using auxiliary force constants and third-order force constants from SSCHA as described in Refs. [55, 58–60]. In the static limit, the peaks of these spectral functions coincide with the eigenvalues of the Hessian of the SSCHA free energy [55]. Here we compare our SSCHA results with standard harmonic calculations performed on the classical structures obtained from the minima of the Born-Oppenheimer energy surface (BOES).

In Supp. Fig. 1 we show the comparison between harmonic and SSCHA phonon band structures for relevant systems (systems that have non-zero superconducting critical temperatures). In the harmonic case, we calculated the phonons using DFPT for the structures that minimize the Born-Oppenheimer energy. In the SSCHA case, we are showing the eigenvalues of the SSCHA auxiliary dynamical matrices for the structures that minimize the total free energy in the self-consistent harmonic approximation.

As we note in the main text, we can see a large softening of the phonon frequencies in the case of the SSCHA structures. This is particularly prominent for optical modes in molecular Cmca-12 phase VI. Another prominent difference is that SSCHA cures the incipient instability in atomic hydrogen at 500 GPa on the $S_0 \rightarrow \Gamma$ line, which leads to the increase of the electron-phonon coupling strength in the harmonic case at this pressure.

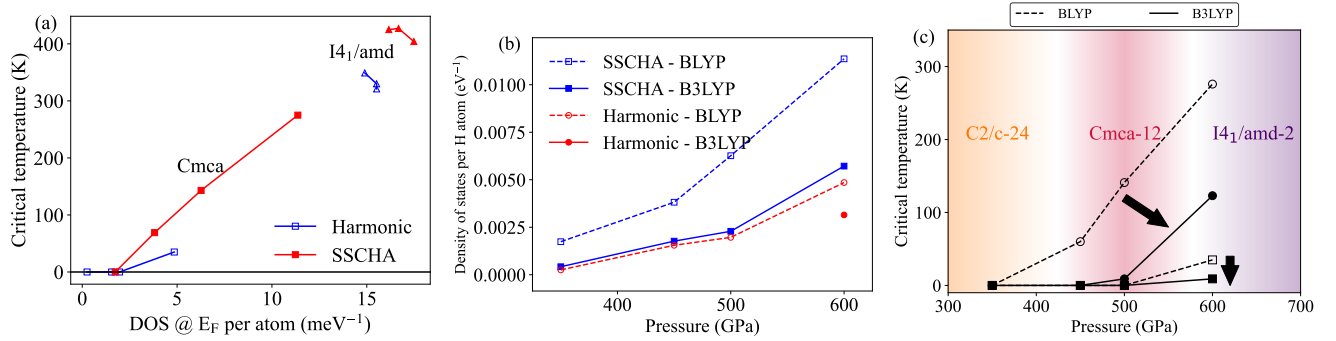
Dependence of the critical temperature on ground state properties

In Supp. Fig. 2 (a) we show the correlation between the superconducting critical temperature T_C and the electronic density of states at the Fermi level in these compounds. As we can see, in molecular phase VI there is a linear correlation between T_C and the electronic density of states. Critical temperature in the figure was calculated using isotropic Migdal-Eliashberg equations with α^2F calculated with full phonon spectral functions in SSCHA case and Gaussian approximation in the harmonic case.

In the atomic phase, it looks like there is a negative correlation between the critical temperature and the electronic density of states. The decrease of the critical temperature in these cases is probably due to the stiffening of the phonon modes with the increased pressure and probably is not connected to the changes in the density of states. This increase in phonon frequencies decreases the electron-phonon coupling strength, which, in turn, reduces T_C . The increase of the electronic density of states does not influence the critical temperature as strongly in this phase since it is far away from the metal-insulator phase transition.

To estimate the error of the calculated density of states using BLYP, we performed B3LYP calculations of the electronic structure on the SSCHA structures that have non-zero critical temperature. The results are shown and compared to DFT in Supp. Fig. 3 (b). As we can see the results with B3LYP drastically reduce the calculated density of states at the Fermi level. Accidentally, B3LYP values agree quite well with BLYP values calculated for harmonic structures. We have also calculated the electronic density of states with B3LYP hybrid functional for 600 GPa harmonic structure (the only one that shows superconductivity in Cmca-12 phase for harmonic structure and Gaussian approximation) and found that it decreases the DOS at the Fermi level significantly.

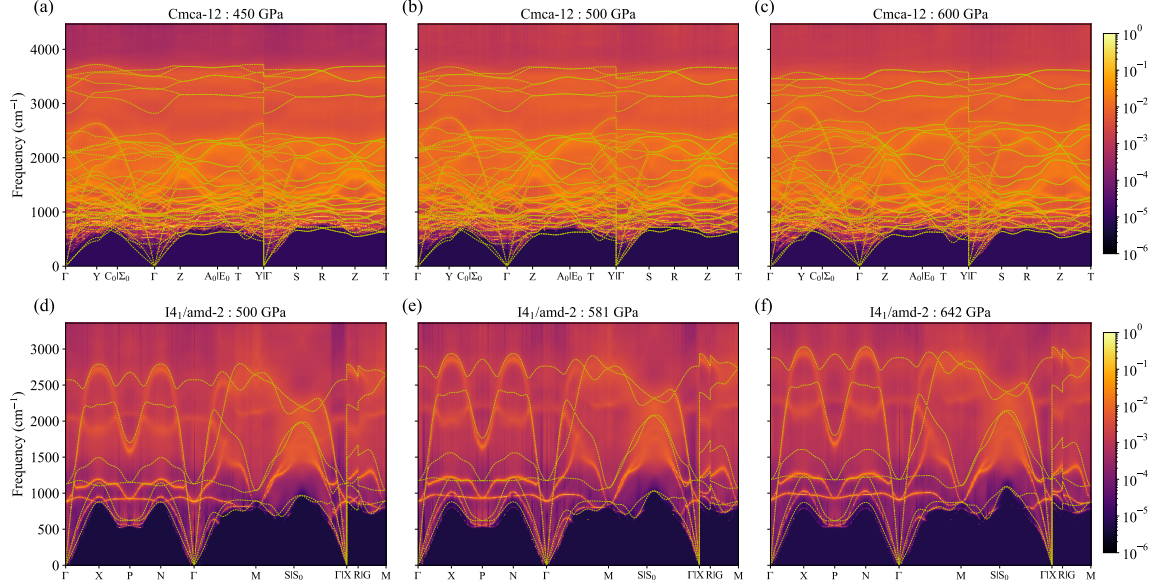
If we assume that the critical temperature is directly proportional to the density of states at the Fermi level we can estimate that the onset of the superconductivity in this phase happens between 450 and 500 GPa. This is the result reported in the main text.



Supplementary Figure 2. a) Critical temperature as a function of the value of the electronic density of states at the Fermi level in molecular phase VI and atomic phase of solid hydrogen. α^2F needed for the estimation of T_C was obtained in the Gaussian approximation for harmonic case and using full phonon spectral function in the SSCHA case. (b) Density of states at the Fermi level of solid hydrogen in Cmca-12 phase (molecular phase VI) calculated with BLYP and B3LYP approximations for the exchange-correlation functional. (c) The changes in the critical temperature in the molecular phase VI (Cmca-12) due to different exchange-correlation functionals. Circles represent results obtained for SSCHA structures with fully anharmonic Eliashberg spectral functions, while squares are for harmonic structures and Eliashberg spectral functions in Gaussian approximation.

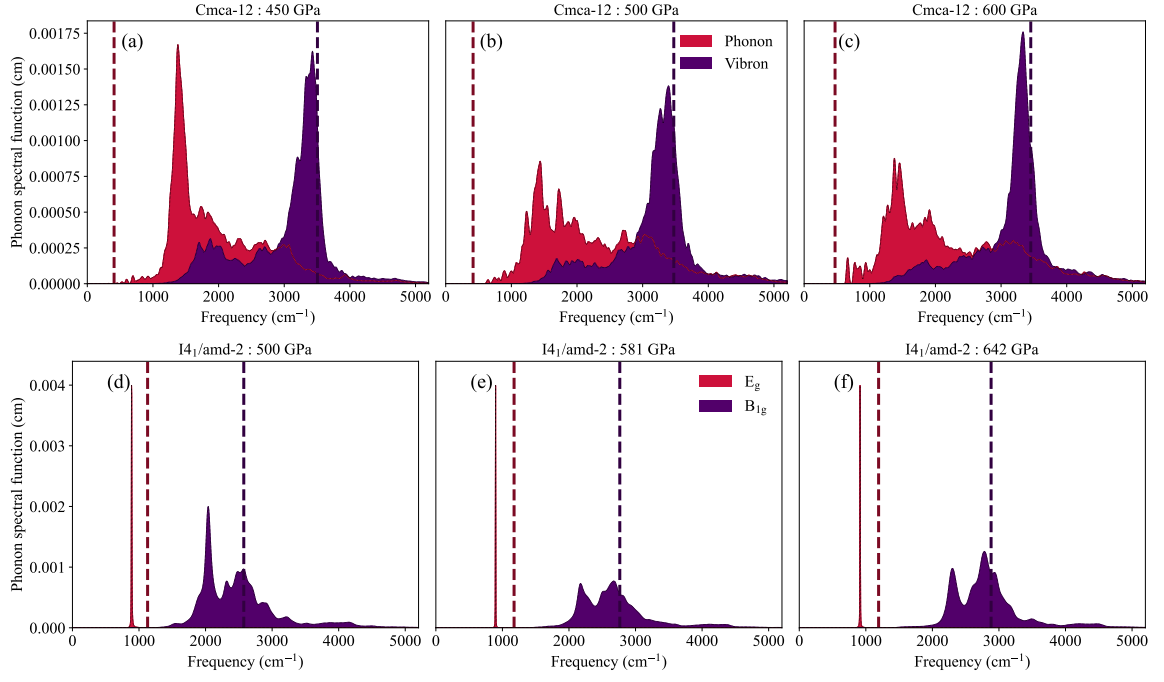
PHONON SPECTRAL FUNCTIONS IN SOLID HYDROGEN

In Supp. Fig. 3 we are showing the phonon lineshapes of solid hydrogen at different pressures and phases along some high symmetry lines in the reciprocal space. Anharmonicity further softens the phonon frequencies for most of the modes, most prominently for the optical phonon modes. There is an obvious closing of the gap between optical modes in the molecular phase of hydrogen.



Supplementary Figure 3. Phonon spectral function $\sigma(\mathbf{q}, \omega) = \sum_{\mu} \sigma_{\mu}(\mathbf{q}, \omega)$ calculated in the no-mode mixing approximation in arbitrary units of solid hydrogen in molecular phase VI (Cmca-12) at (a) 450 GPa, (b) 500 GPa, (c) 600 GPa, and tetragonal $I4_1/amd-2$ atomic phase at (d) 500 GPa, (e) 581 GPa, and (g) 642 GPa. Dashed yellow lines represent eigenvalues of the SSCHA auxiliary dynamical matrices.

In Supp. Fig. 4 we see the phonon mode spectral functions of solid hydrogen at Γ for representative modes. All phases at all pressures show large phonon lineshifts and linewidths.



Supplementary Figure 4. Phonon spectral functions in the no mode mixing approximation in modes basis, $\sigma_\mu(\mathbf{q}, \omega)$, of two representative optical phonon modes at Γ of solid hydrogen in molecular Cmca-12 phase VI at (a) 450 GPa, (b) 500 GPa, (c) 600 GPa, and atomic tetragonal $I4_1/amd-2$ phase at (d) 500 GPa, (e) 581 GPa, and (f) 642 GPa. In figures (d), (e), and (f) we scaled the values of the E_g mode in order to make the figures clearer. Thick dashed vertical lines represent the corresponding frequencies obtained from the auxiliary SSCHA force constants.

Comparison between anharmonic and gaussian Eliashberg spectral functions for SSCHA structures

The solution to the isotropic Migdal-Eliashberg equations gives us the value of the superconducting gap as a function of temperature. The temperature where this value drops to zero we call the critical temperature. To solve isotropic Migdal-Eliashberg equations one only needs the Eliashberg spectral function.

The general definition of the Eliashberg spectral function ($\alpha^2 F(\omega)$) is [38]:

$$\alpha^2 F_{nn'}(\mathbf{k}, \mathbf{q}, \omega) = \frac{N_F}{N_{\mathbf{k}} N_{\mathbf{q}}} \sum_{a,b} d_{n\mathbf{k}, n'\mathbf{k}+\mathbf{q}}^a d_{n'\mathbf{k}+\mathbf{q}, n\mathbf{k}}^b B_{ab}(\mathbf{q}, \omega). \quad (2)$$

Here a, b compactly label atoms in the primitive cell and Cartesian directions, $d_{n\mathbf{k}, n'\mathbf{k}+\mathbf{q}}^a$ is the deformation potential $d_{n\mathbf{k}, n'\mathbf{k}+\mathbf{q}}^a = \langle n\mathbf{k} | \frac{\delta V}{\delta u^a(\mathbf{q})} | n'\mathbf{k} + \mathbf{q} \rangle$, with $|n\mathbf{k}\rangle$ the Kohn-Sham state of band n and wave number \mathbf{k} , and $B_{ab}(\mathbf{q}, \omega)$ is defined as:

$$B_{ab}(\mathbf{q}, \omega) = -\frac{1}{\pi} \text{Im} \mathcal{D}_{ab}(\mathbf{q}, \omega),$$

where $\mathcal{D}_{ab}(\mathbf{q}, \omega)$ is the Fourier transform of the phonon Green's function: $\mathcal{D}_{ab}(\mathbf{q}, t) = -\langle T u_a(\mathbf{q}, t) u_b^*(\mathbf{q}, 0) \rangle$. In order to get the isotropic Eliashberg spectral function from Eq. 2, we average $\alpha^2 F_{nn'}(\mathbf{k}, \mathbf{q}, \omega)$ over the Fermi surface. Once we do that, we obtain:

$$\alpha^2 F(\omega) = \frac{1}{N_{\mathbf{q}}} \sum_{a,b,\mathbf{q}} \Delta^{ab}(\mathbf{q}) B_{ab}(\mathbf{q}, \omega). \quad (3)$$

Here $\Delta^{ab}(\mathbf{q})$ is the shorthand notation for the deformation potential averaged over Fermi surface:

$$\Delta^{ab}(\mathbf{q}) = \frac{1}{N_F N_{\mathbf{k}}} \sum_{n,n',\mathbf{k}} d_{n\mathbf{k}, n'\mathbf{k}+\mathbf{q}}^a d_{n'\mathbf{k}+\mathbf{q}, n\mathbf{k}}^b \delta(\epsilon_{n\mathbf{k}} - \epsilon_F) \delta(\epsilon_{n'\mathbf{k}+\mathbf{q}} - \epsilon_F).$$

In the SSCHA code we use a slightly different definition of the phonon Green's function compared to the definition used here. We define the Green's function with respect to the displacement of the atom scaled by the square root of the atom mass. Additionally, we define the phonon spectral function $\sigma_{ab}(\mathbf{q}, \omega)$ as:

$$\sigma_{ab}(\mathbf{q}, \omega) = -\frac{\omega}{\pi} \text{Im} G_{ab}(\mathbf{q}, \omega) = \frac{\omega}{\pi} \text{Im} \sqrt{m_a m_b} \langle T u_a u_b^* \rangle(\mathbf{q}, \omega) = \omega \sqrt{m_a m_b} B_{ab}(\mathbf{q}, \omega).$$

This result is given in the atomic Cartesian basis, but we can cast this result in the no mode mixing approximation. In this approximation atomic displacements are projected onto phonon modes ($\sigma_{ab}(\mathbf{q}, \omega) = \sum_{\mu} e_{\mu}^a(\mathbf{q}) e_{\mu}^{b*}(\mathbf{q}) \sigma_{\mu}(\mathbf{q}, \omega)$). This no mode mixing approximation is usually very good in describing phonon spectral functions.

Usually, the mode projected phonon spectral function $\sigma_{\mu}(\mathbf{q})$ is approximated with:

$$\sigma_{\mu}^h(\mathbf{q}, \omega) = \frac{1}{2} [\delta(\omega + \omega_{\mu}^h(\mathbf{q})) + \delta(\omega - \omega_{\mu}^h(\mathbf{q}))]. \quad (4)$$

Then Dirac delta $\delta(\omega - \omega_{\mu}^h(\mathbf{q}))$ is approximated with a Gaussian centered at the value of harmonic phonon frequency $\omega_{\mu}^h(\mathbf{q})$ and the fixed width which is the same for each phonon mode (in our calculation we took this smearing parameter to be 10 cm^{-1}).

SSCHA however, allows us to calculate the third-order interatomic force constants, in addition to the crystal structure and second order force constants renormalized by anharmonicity. Using these third-order force constants we can explicitly calculate the phonon mode spectral function $\sigma_{\mu}(\mathbf{q}, \omega)$ (in the diagonal dynamical bubble approximation). It is defined as [53, 55]:

$$\sigma_{\mu}(\mathbf{q}, \omega) = \frac{1}{2\pi} \left[\frac{-\text{Im} \mathcal{Z}_{\mu}(\mathbf{q}, \omega)}{[\omega - \text{Re} \mathcal{Z}_{\mu}(\mathbf{q}, \omega)]^2 + [\text{Im} \mathcal{Z}_{\mu}(\mathbf{q}, \omega)]^2} + \frac{\text{Im} \mathcal{Z}_{\mu}(\mathbf{q}, \omega)}{[\omega + \text{Re} \mathcal{Z}_{\mu}(\mathbf{q}, \omega)]^2 + [\text{Im} \mathcal{Z}_{\mu}(\mathbf{q}, \omega)]^2} \right]. \quad (5)$$

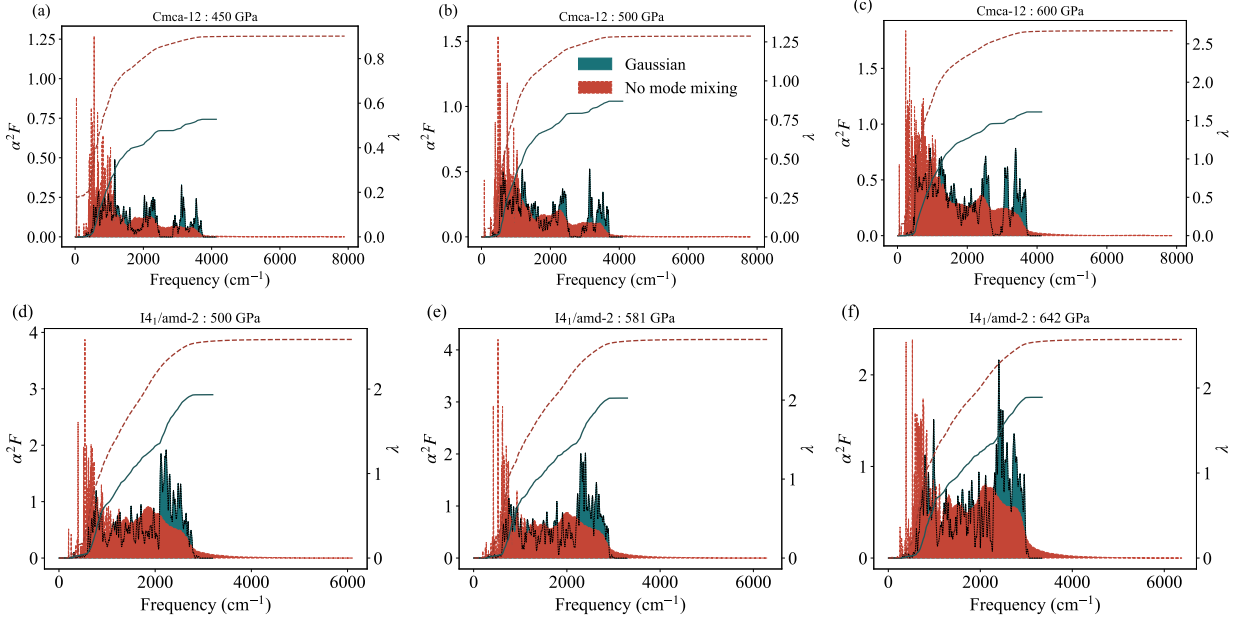
Here $\mathcal{Z}_{\mu}(\mathbf{q}, \omega) = \sqrt{\omega_{\mu}^2(\mathbf{q}) + \Pi_{\mu}(\mathbf{q}, \omega)}$, where $\Pi_{\mu}(\mathbf{q}, \omega)$ is the phonon self-energy due to phonon-phonon interaction in the bubble approximation:

$$\begin{aligned} \Pi_{\mu}(\mathbf{q}, \omega) &= \frac{1}{N_{\mathbf{k}}} \sum_{\mathbf{k}_1, \nu} \sum_{\mathbf{k}_2, \rho} \sum_{\mathbf{G}} \delta_{\mathbf{G}, \mathbf{q} + \mathbf{k}_1 + \mathbf{k}_2} |D_{\mathbf{q}\mathbf{k}_1\mathbf{k}_2}^{\mu\nu\rho}|^2 \times \\ &\times \frac{\hbar}{4\omega_{\nu}(\mathbf{k}_1)\omega_{\rho}(\mathbf{k}_2)} \left(\frac{(\omega_{\nu}(\mathbf{k}_1) - \omega_{\rho}(\mathbf{k}_2))(n_{\nu}(\mathbf{k}_1) - n_{\rho}(\mathbf{k}_2))}{(\omega_{\nu}(\mathbf{k}_1) - \omega_{\rho}(\mathbf{k}_2))^2 - \omega^2} - \frac{(\omega_{\nu}(\mathbf{k}_1) + \omega_{\rho}(\mathbf{k}_2))(n_{\nu}(\mathbf{k}_1) + n_{\rho}(\mathbf{k}_2) + 1)}{(\omega_{\nu}(\mathbf{k}_1) + \omega_{\rho}(\mathbf{k}_2))^2 - \omega^2} \right). \quad (6) \end{aligned}$$

Here $n_{\mu}(\mathbf{q})$ is the Bose-Einstein occupation factor for the phonon mode with frequency $\omega_{\mu}(\mathbf{q})$ and $D_{\mathbf{q}\mathbf{k}_1\mathbf{k}_2}^{\mu\nu\rho}$ is the Fourier transform of the third-order force constants (including the scaling with atom masses). An important note is that $\omega_{\mu}(\mathbf{q})$ are calculated from eigenvalues of the auxiliary SSCHA force constants. The same definition of the spectral function was used in Fig. 2 of the main text. As we can see this quantity is actually temperature dependent (through $n_{\mu}(\mathbf{q})$) and in principle should be recalculated at each temperature. Here, however, we only calculate it at 0 K ($n_{\mu}(\mathbf{q}) = 0$ always) and the only processes accounted for are the annihilations of two phonons (second term in the parenthesis). We did perform calculations for atomic hydrogen at 500 GPa using spectral functions calculated at 300 K and the results for the critical temperature did not change. Another important detail that we would like to stress is that the phonon spectral functions calculated here come purely from the phonon-phonon interaction. We justify this with the fact that for the temperature range of interest (around 100 K), phonon linewidths due to the phonon-phonon interaction are orders of magnitude larger than the phonon linewidths due to the electron-phonon interaction for most of the phonon modes.

In Supp. Figure 5 we compare results for the Eliashberg spectral function $\alpha^2 F(\omega)$ calculated using Eq. 4 but with phonon frequencies and polarization vectors coming from the SSCHA auxiliary force constants, not the harmonic phonons, (labeled Gaussian) and Eq. 5 with the phonon self energy from Eq. 6 (labeled Anharmonic). This Gaussian approach is the one that has been used so far in the literature to estimate the anharmonic renormalization of the Eliashberg function. Thus, in both cases, we used properties obtained with SSCHA (structure and interatomic force constants). Treating phonon spectral function in the dynamical bubble approximation further softens phonon modes. In molecular phase VI, this leads to the complete closing of the vibron-phonon gap. This softening mostly increases the final electron-phonon coupling strength. Additionally, in the ‘‘no mode mixing’’ calculation we can see a longer tail at higher frequencies which is a consequence of the phonon-phonon interaction that includes the annihilation of two phonon modes.

To gauge the influence of this change of the Eliashberg spectral function on the superconductivity we calculated critical temperature using the isotropic Migdal-Eliashberg equation. Results for different calculations are shown in



Supplementary Figure 5. Eliashberg spectral function and electron-phonon coupling constant of solid hydrogen in molecular Cmca-12 phase VI at (a) 450 GPa, (b) 500 GPa, (c) 600 GPa and atomic tetragonal I4₁/amd-2 phase at (d) 500 GPa, (e) 581 GPa and (f) 642 GPa. Gaussian represents results where we used SSCHA structures and second order force constants (auxiliary force constants), but calculated $\alpha^2 F$ by using Eq. 4 for definition of spectral function (smearing in Gaussian function of 10 cm⁻¹). Anharmonic represents results where we used SSCHA structures and second order force constants (auxiliary force constants), but calculated $\alpha^2 F$ by using Eq. 5 for definition of spectral function.

Supp. Table I. The “Anharmonic” calculations consistently show higher critical temperature in both phases. This is mainly due to the softening of the phonon modes due to the anharmonicity. Additionally, we calculate the Eliashberg spectral function in Gaussian approximation using free energy Hessian phonons, see Supp. Fig. 6. These calculations consistently give higher critical temperature which is again a consequence of the softening of the phonon modes in this approximation. Calculations with Hessian phonons give larger T_{CS} compared to calculations done with realistic broadening in no mode mixing approximation, but still lower than T_C estimated in the mode mixing approach. This is a good argument for using Hessian phonons to calculate critical temperatures.

From the mode projected spectral functions $\sigma_\mu(\mathbf{q}, \omega)$ one can get the Cartesian based spectral function with $\sigma_{ab}(\mathbf{q}, \omega) = \sum_\mu e_\mu^a(\mathbf{q}) e_\mu^{b*}(\mathbf{q}) \sigma_\mu(\mathbf{q}, \omega)$, where $e_\mu(\mathbf{q})$ is the eigenvector of the phonon with branch μ and wave vector \mathbf{q} . However, one can avoid making the no mode mixing approximation, which is made in Eq. 6, by calculating the full matrix of the phonon self energy:

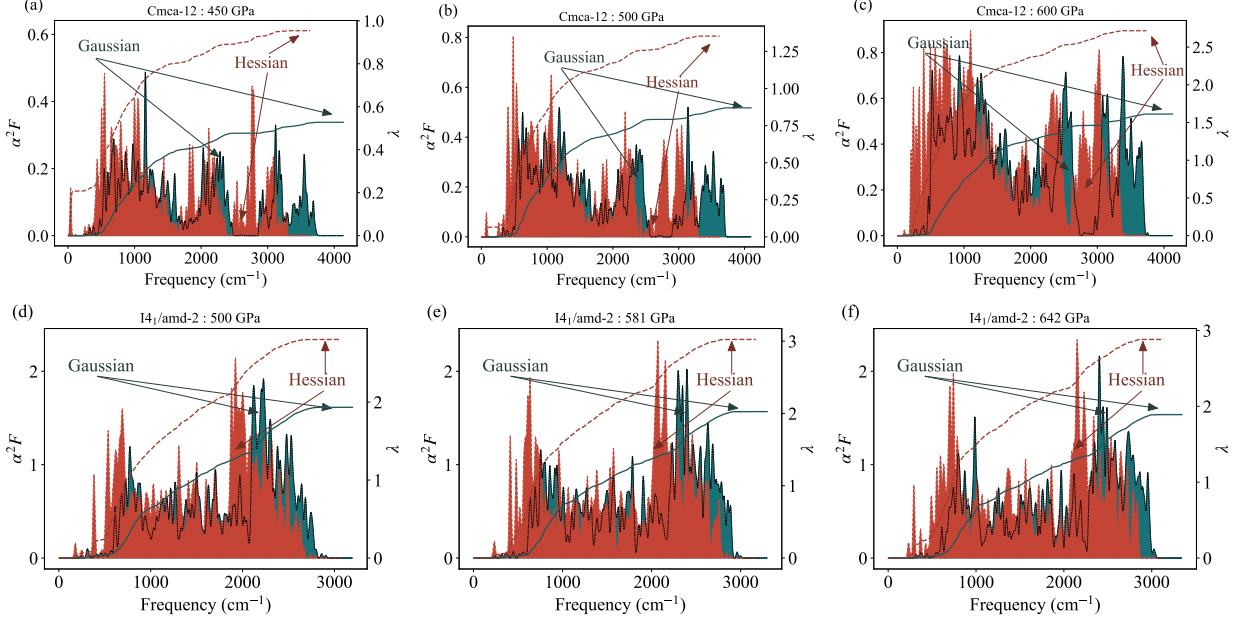
$$\begin{aligned} \Pi_{\mu\mu'}(\mathbf{q}, \omega) &= \frac{1}{N_{\mathbf{k}}} \sum_{\mathbf{k}_1, \nu} \sum_{\mathbf{k}_2, \rho} \sum_{\mathbf{G}} \delta_{\mathbf{G}, \mathbf{q} + \mathbf{k}_1 + \mathbf{k}_2} D_{\mathbf{q}\mathbf{k}_1\mathbf{k}_2}^{\mu\nu\rho} D_{-\mathbf{k}_1 - \mathbf{k}_2 - \mathbf{q}}^{\nu\rho\mu'} \times \\ &\times \frac{\hbar}{4\omega_\nu(\mathbf{k}_1)\omega_\rho(\mathbf{k}_2)} \left(\frac{(\omega_\nu(\mathbf{k}_1) - \omega_\rho(\mathbf{k}_2))(n_\nu(\mathbf{k}_1) - n_\rho(\mathbf{k}_2))}{(\omega_\nu(\mathbf{k}_1) - \omega_\rho(\mathbf{k}_2))^2 - \omega^2} - \frac{(\omega_\nu(\mathbf{k}_1) + \omega_\rho(\mathbf{k}_2))(n_\nu(\mathbf{k}_1) + n_\rho(\mathbf{k}_2) + 1)}{(\omega_\nu(\mathbf{k}_1) + \omega_\rho(\mathbf{k}_2))^2 - \omega^2} \right). \end{aligned} \quad (7)$$

Plugging this self-energy in the Dyson equation one can get a complete phonon Green’s function:

$$G_{\mu\mu'}(\mathbf{q}, \omega) = [\omega^2 \delta_{\mu\mu'} - D_{\mu\mu'}(\mathbf{q}) - \Pi_{\mu\mu'}(\mathbf{q}, \omega)]^{-1}.$$

Here $D_{\mu\mu'}(\mathbf{q})$ is the auxiliary SSCHA dynamical matrix in the mode basis (it is diagonal in this basis). Since we are taking the inverse in the equation above, we in essence are mixing self-energies of different phonon branches. The full phonon spectral function is then straightforwardly calculated as $\sigma_{\mu\mu'}(\mathbf{q}, \omega) = -\frac{\omega}{\pi} \text{Im} G_{\mu\mu'}(\mathbf{q}, \omega)$, which can later be projected onto the Cartesian basis:

$$\sigma_{ab}(\mathbf{q}, \omega) = \sum_{\mu, \mu'} e_\mu^a(\mathbf{q}) e_{\mu'}^{b*}(\mathbf{q}) \sigma_{\mu\mu'}(\mathbf{q}, \omega). \quad (8)$$



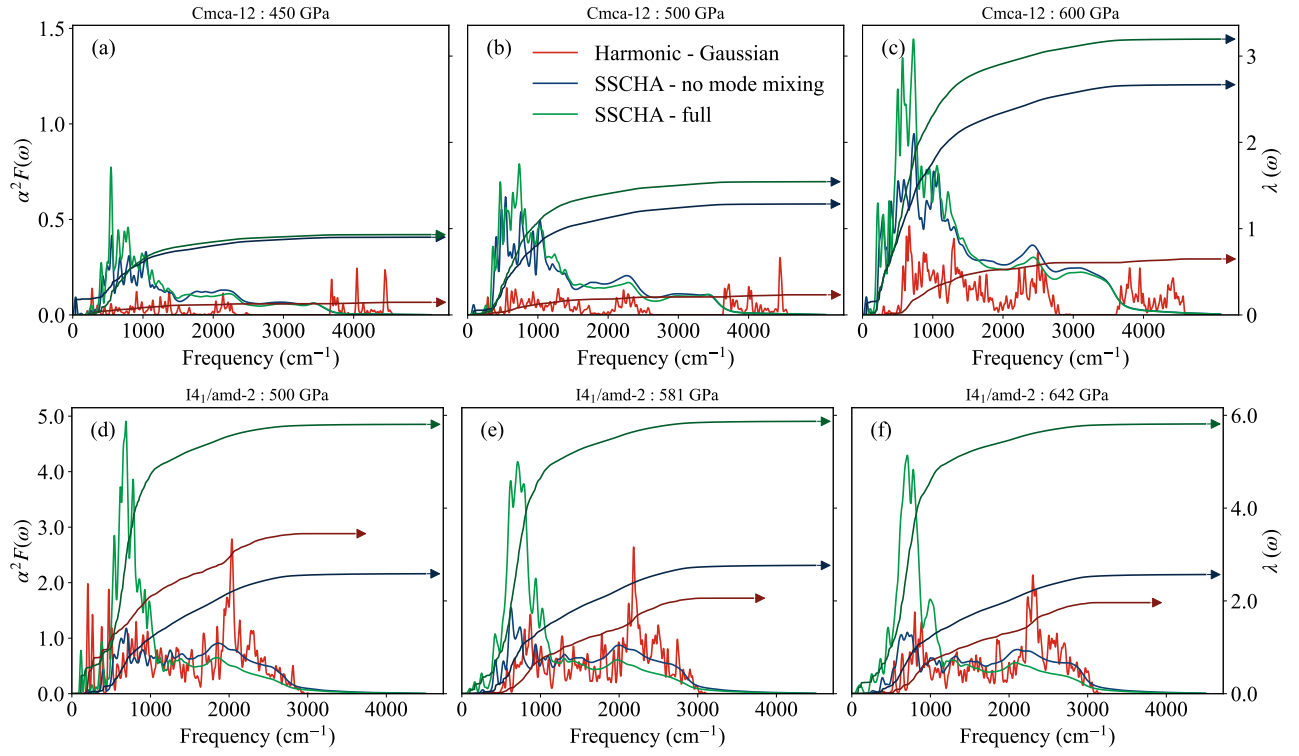
Supplementary Figure 6. Eliashberg spectral function and electron-phonon coupling constant of solid hydrogen in molecular Cmca-12 phase VI at (a) 450 GPa, (b) 500 GPa, (c) 600 GPa and atomic tetragonal $I4_1/amd-2$ phase at (d) 500 GPa, (e) 581 GPa and (f) 642 GPa. Gaussian represents results where we used SSCHA structures and second order force constants (auxiliary force constants), but calculated $\alpha^2 F$ by using Eq. 4 for definition of spectral function (smearing in Gaussian function of 10 cm^{-1}). Hessian represents results where we used SSCHA structures and eigenvalues from free energy Hessian and calculated $\alpha^2 F$ by using Eq. 4 for definition of spectral function.

Finally, we calculate the critical temperature in the atomic phase using the full spectral function, see Supp. Fig. 7. We find a large increase in the critical temperature. The analysis of why the critical temperature increases in mode mixing approach is complicated due to the fact that we sum over a product of deformation potentials and spectral functions, see Eq. 3. This means that if there is no large change in phonon spectral functions (as we can see from Supp. Fig. 8), the increase comes from the intricate relationship between elements of deformation potentials and phonon spectral functions.

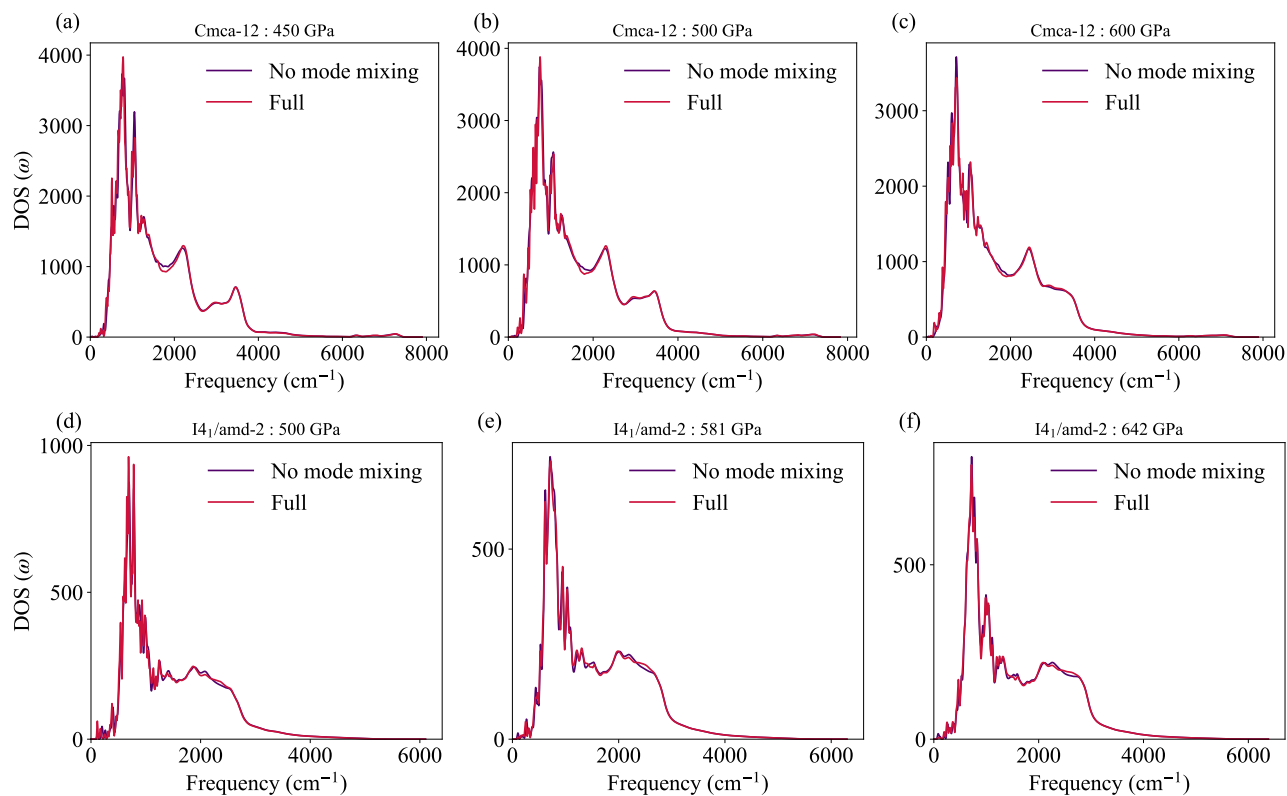
T_C	molecular Cmca-12			atomic $I4_1/amd-2$		
	450 GPa	500 GPa	600 GPa	500 GPa	581 GPa	642 GPa
Gaussian - Harmonic	0 K	0 K	35 K	349 K	330 K	321 K
Gaussian - Auxiliary	19 K	83 K	219 K	313 K	334 K	322 K
Gaussian - Hessian	52 K	129 K	268 K	356 K	376 K	370 K
Anharmonic - no mode mixing	44 K	118 K	250 K	337 K	357 K	347 K
Anharmonic - full	60 K	141 K	276 K	404 K	427 K	425 K

Supplementary Table I. Superconducting critical temperature in solid hydrogen molecular VI Cmca-12 and atomic $I4_1/amd-2$ phases. These results are obtained with BLYP exchange-correlation DOS, which is why differ from Fig. 1. Harmonic results are obtained using DFT structures, harmonic phonons with Eliashberg spectral function calculated using Eq. 4. Gaussian results are obtained using SSCHA structures, SSCHA auxiliary phonons with Eliashberg spectral function calculated using Eq. 4. Anharmonic results are obtained using SSCHA structures, SSCHA auxiliary phonons with Eliashberg spectral function calculated using Eq. 5 and Eq. 7.

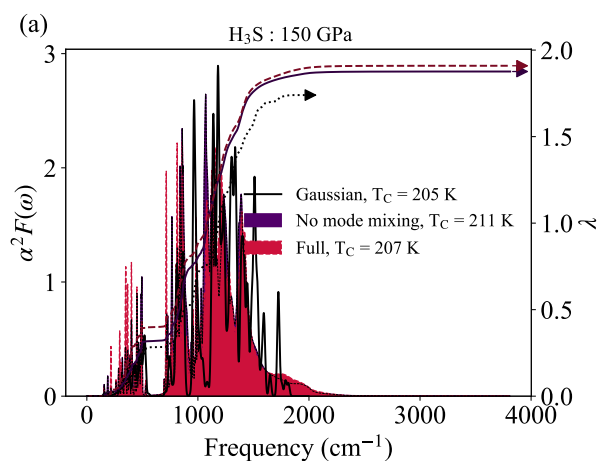
To make sure that these results are reliable, we also calculated the critical temperature of H_3S at 150 GPa using this method. The simple Gaussian approximation already gives a very good estimation of the critical temperature in this system and the new approach including phonon spectral functions should not change it [26]. This is what we see in our calculations, where anharmonic phonon spectral functions have a limited effect on critical temperature, see Supp. Fig. 9.



Supplementary Figure 7. Eliashberg spectral function $\alpha^2 F(\omega)$ and integrated electron-phonon coupling constant $\lambda(\omega)$ of solid hydrogen in molecular Cmca-12 phase VI at (a) 450 GPa, (b) 500 GPa, (c) 600 GPa, and atomic tetragonal I4₁/amd-2 phase at (d) 500 GPa, (e) 581 GPa, and (f) 642 GPa calculated in the SSCHA using the spectral function calculated fully and in the no mode mixing approximation, and in the harmonic case using Gaussian method.



Supplementary Figure 8. Phonon density of states calculated with the full phonon spectral functions and with the ones obtained in the no mode mixing approximation for the molecular Cmca phase of solid hydrogen at a) 450 GPa, b) 500 GPa, c) 600 GPa, and the atomic phase of solid hydrogen at d) 500 GPa, e) 581 GPa and f) 642 GPa.



Supplementary Figure 9. Eliashberg spectral function of H₃S at 150 GPa calculated with three different methods.